ARTICLES
PUBLISHED ONLINE: 11 APRIL 2010 | DOI: 10.1038/NMAT2742
nature materials

Free-floating ultrathin two-dimensional crystals from sequence-specific peptoid polymers

Ki Tae Nam[1], Sarah A. Shelby[1], Philip H. Choi[1], Amanda B. Marciel[1], Ritchie Chen[1], Li Tan[1], Tammy K. Chu[1], Ryan A. Mesch[1], Byoung-Chul Lee[1], Michael D. Connolly[1], Christian Kisielowski[2] and Ronald N. Zuckermann[1]*

The design and synthesis of protein-like polymers is a fundamental challenge in materials science. A biomimetic approach is to explore the impact of monomer sequence on non-natural polymer structure and function. We present the aqueous self-assembly of two peptoid polymers into extremely thin two-dimensional (2D) crystalline sheets directed by periodic amphiphilicity, electrostatic recognition and aromatic interactions. Peptoids are sequence-specific, oligo-*N*-substituted glycine polymers designed to mimic the structure and functionality of proteins. Mixing a 1:1 ratio of two oppositely charged peptoid 36mers of a specific sequence in aqueous solution results in the formation of giant, free-floating sheets with only 2.7 nm thickness. Direct visualization of aligned individual peptoid chains in the sheet structure was achieved using aberration-corrected transmission electron microscopy. Specific binding of a protein to ligand-functionalized sheets was also demonstrated. The synthetic flexibility and biocompatibility of peptoids provide a flexible and robust platform for integrating functionality into defined 2D nanostructures.

Proteins are information-rich polymers that fold hierarchically into precise three-dimensional functional structures encoded by a specific monomer sequence. Despite ongoing advances, it is still a significant challenge for synthetic polymers to form atomically defined structures and reach the same level of complexity and functionality that proteins attain. However, the processability and robustness of synthetic polymers and their capacity to form periodic nanoscale structures over macroscopic length scales are advantages over polypeptide-based approaches. Although macromolecules[1] and multi-block copolymers[2] can achieve order on the nanometre scale, the synthetic flexibility to functionalize precise atomic locations and to incorporate complex sequence information into current platforms is limited. In an ongoing effort to extend the fundamental understanding of protein structure to non-natural systems, we have designed a class of peptoid polymers to fold like proteins and assemble into defined nanostructures. We have identified specific sequences of non-biological peptoid polymer chains that crystallize into extremely thin sheets under physiological conditions.

Two-dimensional crystalline materials are a fundamentally important geometry for control of surface properties, device fabrication, membrane-based separations and their unique electronic properties. The predominant routes to prepare these materials rely on using liquid/liquid, liquid/solid and liquid/air interfaces, which act as templates[3–5]. Chemical synthesis[6] and exfoliation[7] from layered crystals have also been used to fabricate 2D nanostructures. However, there are only a few examples[8–11] of such materials prepared by solution self-assembly. In 1957, polyethylene was observed to crystallize into thin platelets from solution[12]. Since then, certain homopolymers have been shown to form 2D crystals in which the chains are folded back and forth perpendicular to the planar surface[13–15]. As these homopolymers have no sequence information, there is no chemical distinction between the surface and the interior, severely limiting the ability to functionalize or engineer these materials. Polypeptide-based 2D structures were hypothesized to exist as early as 1975 (ref. 16) and later demonstrated experimentally by the observation of macroscopic membranes[8,17]. However, laterally extended (planar aspect ratio close to 1:1), untwisted, flat, 2D polypeptide crystals have not been observed. Peptides engineered as nanomaterials tend to form one-dimensional nanostructures[18–20] that are often twisted because of structural factors such as chirality.

Peptoids are non-natural, bio-inspired, information-rich polymers that allow unprecedented control over monomer sequence, monomer chemistry and main-chain length[21–26]. The structure of a peptoid monomer (an *N*-substituted glycine) differs from a natural amino acid only in that the side chains are appended to the amide nitrogen rather than the alpha carbon. Like proteins, peptoids are sequence-specific heteropolymers. They exhibit potent biological activities, fold into specific structures[24,25] and demonstrate resistance to proteolysis. In contrast to polypeptides, peptoids lack both chirality and a hydrogen-bond donor in their backbone. This allows for a simplicity of design that is suited to the study of different folding principles. An important feature of peptoids is that the accessible side-chain diversity is enormous, as the solid-phase submonomer method of synthesis is highly efficient and uses primary amines as synthons[26]. These attributes make peptoids a versatile tool kit for studying the assembly of precisely ordered protein mimetic materials.

Analysis of protein structure reveals some design principles that can be applied to the folding of non-natural polymers. Arguably, the dominant driving force involved in the folding of polypeptide chains into protein structures in aqueous solution is the burial of hydrophobic amino-acid residues in an interior core and the exposure of the hydrophilic side chains to solvent[27]. Study of folded proteins and self-assembling peptides has shown that the sequence pattern and periodicity of polar and nonpolar residues are the primary determinants of secondary structure[28,29].

[1]Molecular Foundry; [2]National Center for Electron Microscopy, Lawrence Berkeley National Laboratory, Berkeley, California 94720, USA.
*e-mail: rnzuckermann@lbl.gov.

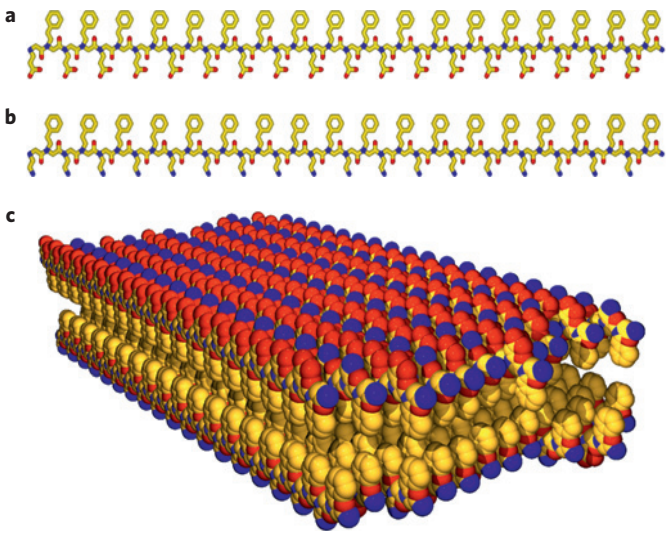

Figure 1 | Two-dimensional crystalline sheets formed from two oppositely charged peptoid polymers. Atomic colour scheme: carbon, yellow; nitrogen, blue; oxygen, red. **a**, Chemical structure of a negatively charged periodic amphiphilic peptoid, $(Nce\text{–}Npe)_{18}$. **b**, Chemical structure of a positively charged periodic amphiphilic peptoid, $(Nae\text{–}Npe)_{18}$ **c**, Molecular model of the sheets assembled from $(Nae\text{–}Npe)_{18}$ and $(Nce\text{–}Npe)_{18}$. The modelled conformation shows that hydrophobic groups face each other in the interior of the sheet and oppositely charged hydrophilic groups are alternating and surface-exposed.

We systematically introduced simple periodic sequence patterns of polar and nonpolar monomers into a fixed-length polypeptoid chain to study the impact of sequence on self-assembly. We also segregated like charges on complementary strands to include electrostatic interactions between peptoid chains. Electrostatic interactions have been used to induce order in many self-assembly systems such as polyelectrolyte multilayers[30,31], nanoparticles, catanionic amphiphiles[32], nucleic-acid delivery vehicles[23,33], ionic self-complementary peptides[34] and counterion–lipid systems[35].

To systematically vary the ratio and spacing of hydrophobic and electrostatic functional groups, a minimalist monomer set was chosen consisting of two types: polar and nonpolar. A simple aromatic monomer, *N*-(2-phenethyl) glycine (Npe), was chosen for the hydrophobic monomer. A pair of ionic side chains was chosen for the polar monomers, *N*-(2-aminoethyl) glycine (Nae) and *N*-(2-carboxyethyl) glycine (Nce). The main-chain length was fixed to 36 monomers so that a small library of peptoids with different repeating sequence motifs could be made. There are a limited number of regular, periodic sequence patterns of two monomer types possible, so we focused on the simplest cases: twofold, threefold and fourfold sequence periodicities. For each periodicity, a complementary pair of sequences was made: positively charged and negatively charged. Thus, the twofold [$(Nae\text{–}Npe)_{18}$ and $(Nce\text{–}Npe)_{18}$] (Fig. 1a and b), threefold [$(Nae\text{–}Npe\text{–}Npe)_{12}$ and $(Nce\text{–}Npe\text{–}Npe)_{12}$] and fourfold [$(Nae\text{–}Npe\text{–}Npe\text{–}Npe)_9$ and $(Nce\text{–}Npe\text{–}Npe\text{–}Npe)_9$] sequence pairs were synthesized (Supplementary Table S1).

Neither the threefold periodic peptoids, $(Nae\text{–}Npe\text{–}Npe)_{12}$ and $(Nce\text{–}Npe\text{–}Npe)_{12}$, nor fourfold peptoids, $(Nae\text{–}Npe\text{–}Npe\text{–}Npe)_9$ and $(Nce\text{–}Npe\text{–}Npe\text{–}Npe)_9$, formed well-defined nanostructures on mixing (Supplementary Fig. S1). Interestingly, the threefold periodic peptoids formed uniform spherical assemblies, similar in size and morphology to cationic peptoid/DNA complexes[23]. The more hydrophobic fourfold peptoids formed extended amorphous aggregates. However, the twofold periodic peptoids, $(Nae\text{–}Npe)_{18}$ and $(Nce\text{–}Npe)_{18}$, composed of alternating polar and nonpolar residues (Fig. 1a,b) assembled into 2D structures when mixed. Sequence periodicity is clearly a major determinant of peptoid nanostructure morphology.

For the assembly of sheets, $(Nae\text{–}Npe)_{18}$ and $(Nce\text{–}Npe)_{18}$ were each dissolved in the same aqueous buffer at the same concentration (10–100 μM), and an equal volume of the former was added rapidly to the latter at room temperature. Fluorescence microscopy using an extrinsic environmentally sensitive dye showed that sheets are free-floating and robust in aqueous solution and form in high yield (Fig. 2a,b and Supplementary Movie S1). Typical sheet edge length is between tens to hundreds of micrometres and in some cases up to two millimetres. The persistence of the sheet structure was observed between pH 2 and 13 and in the presence of organic solvents (up to 50% acetonitrile). Interestingly, scanning electron microscopy (SEM) reveals that two opposite sides of most sheets have very straight edges whereas the other two sides are rough, suggesting that the peptoids are aligned in one direction along the sharp edge (Fig. 2c). Atomic force microscopy (AFM) analysis shows that the sheets are very flat and uniform with a thickness of 2.7 nm (Fig. 2d).

The molecular structure of the sheet was analysed with aberration-corrected transmission electron microscopy (TEM; Fig. 3) and X-ray diffraction (XRD; Fig. 4a). The peptoid sheets are crystalline according to XRD. For powder XRD analysis, solid samples were prepared by centrifuging out the sheets. Three equally spaced peaks (Fig. 4a) indicate a sheet thickness of 27 Å and that the sheets are stacked on top of each other in a lamellar structure (as a result of the XRD sample preparation). Importantly, in solution, the individual sheets of 2.7 nm thickness are not stacked but free-floating as observed by optical microscopy, SEM and AFM (Fig. 2). They are one of the thinnest known 2D organic crystalline materials with an extremely high aspect ratio (area/thickness ratio $>10^9$ nm). The strong peak at $q = 1.4$ is due to the alignment of peptoid chains, with a spacing of 4.5 Å between the peptoids. Further analysis with grazing-incidence XRD provided clear evidence that the peak at 4.5 Å results from in-plane ordering, normal to the sheet's thickness (Supplementary Fig. S2). The 4.5 Å spacing is close to the typical 4.7 Å seen in peptides interlinked by hydrogen bonding in beta sheets[19]. We believe that the peak at 5.3 Å is due to the ordering of the aromatic side chains within the hydrophobic core. This value is similar to the 5.1 Å mean distance between phenyl ring centroids in the edge-face configuration of aromatic side chains in proteins[36]. The 3.6 Å spacing corresponds to the distance between each residue along the chain direction in an extended conformation, slightly larger than the 3.5 Å observed in a peptidic beta sheet. The diffraction at 2.8 Å ($q = 2.25$ Å^{-1}) may result from the (110) lattice plane given an orthorhombic cell ($a = 4.5, b = 3.6, c = 27$ Å). Solution X-ray analyses of free-floating sheets at 5 mg ml^{-1} in aqueous solution do not show the lamellar peaks at $q = 0.23$ Å^{-1}, yet they still show the inter-chain spacing peak at 4.5 Å (Supplementary Fig. S3). A broad, non-Bragg scattering peak centred at $q = 0.27$ Å^{-1} was observed, and was fitted to a model that describes the scattering of an extended planar structure of 3 nm thickness[37].

To determine the molecular structure, we employed a new technique for soft-matter imaging, aberration-corrected TEM (TEAM 0.5) (ref. 38). Direct observation of individual polymer chains (not possible with the conventional transmission electron microscope, Supplementary Fig. S4), revealed unprecedented detail about the structural organization of the peptoid sheet. Direct imaging of a peptoid sheet on a holey carbon grid clearly resolved individual peptoid chains and showed that peptoids are ordered along the direction of the sheet's sharp edge (Fig. 3). Remarkably, the peptoid backbones are nearly straight and their orientations are correlated throughout the structure despite the non-biological analysis condition (for example, high vacuum, electron beam irradiation). This indicates that the peptoids are fully extended, presumably in the all-*trans* conformation, which results in amphiphilic display of side chains along the entire

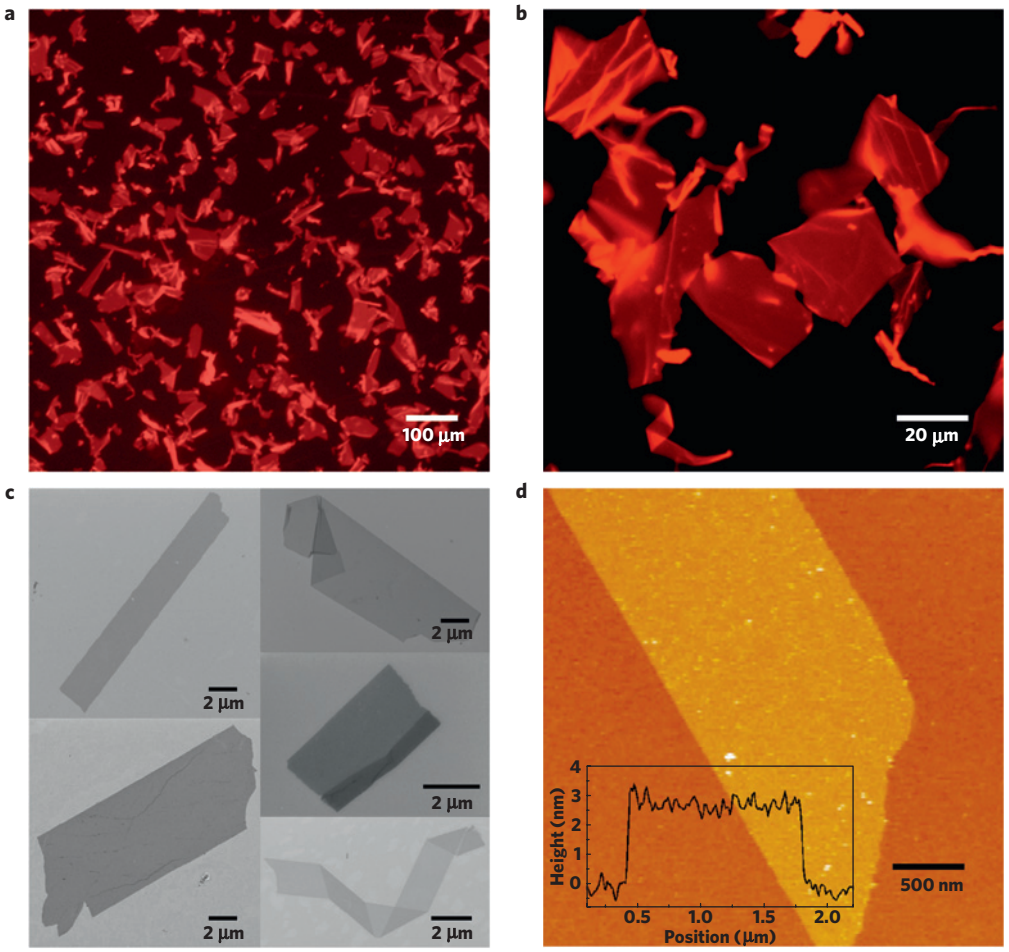

Figure 2 | Imaging of 2D crystalline sheets assembled from periodic amphiphilic peptoid polymers. In typical conditions, 0.1 mM of $(Nae–Npe)_{18}$ and $(Nce–Npe)_{18}$ were mixed in Tris–HCl buffer (pH 9.0, 100 mM). **a**, Fluorescent optical microscope image of sheets stained with Nile Red (1 μM) that are free-floating in aqueous solution. **b**, Fluorescent optical microscope image of individual sheets. **c**, SEM images of sheets on Si substrate. **d**, Height-mode AFM image of a sheet (*Z* range: 20 nm).

peptoid chain (as in Fig. 1). A recent NMR study[39] of peptoid conformation showed that the *trans* conformation of the backbone amide bonds in peptoids is slightly more favourable in solution than the *cis* conformation with the measured rate for *cis/trans* isomerization between 0.1 and 0.3 s^{-1}. The measured inter-chain distance between aligned peptoids from the TEM image is 4.5 Å, which matches well with the observed *d* spacing from XRD and electron diffraction analysis (Supplementary Fig. S5) using a conventional transmission electron microscope. The robustness of peptoid sheets against electron radiation is presumably due to the crystallinity of the aromatic side chains. Phenyl groups are known to be relatively stable[40] to radiation damage because of bond delocalization. The small 2.7 nm thickness also decreases radiation damage mainly caused by electron bombardment. Direct imaging of peptoid strands provides a new paradigm for the analysis of ordered soft materials.

The molar composition of $(Nae–Npe)_{18}$ and $(Nce–Npe)_{18}$ in the sheet structure is 1:1. The sheets were formed in different mixing ratios: 2:1, 1:1 and 1:2 of $(Nae–Npe)_{18}$ and $(Nce–Npe)_{18}$. After separating the sheets from any soluble peptoids, they were dissolved in 50:50 acetonitrile/water (v/v) with the addition of HCl (final 5 mM) and analysed by high-performance liquid chromatography. Regardless of the initial ratio of the two peptoids, the composition of the sheet was always 1:1 (Fig. 4c and Supplementary Fig. S6).

The critical sheet-forming concentration is between 0.1 μM and 1.0 μM, and the relative ratio of the two peptoids significantly affects sheet population (Fig. 4d). The largest number of sheets was observed when the concentrations of $(Nae–Npe)_{18}$ and $(Nce–Npe)_{18}$ were equal. Sheet formation was observed between pH 5 and 12. When both oppositely charged peptoids contained a similar number of charges, around pH 8–9, the sheet population was the highest. The charge density of peptoids at a given pH can be estimated from the acid–base titration curve of the two individual peptoids in aqueous solution (Supplementary Fig. S7). Below pH 7 and above pH 10, the charge imbalance between the two peptoids becomes large, thus decreasing sheet formation. To study the role of the electrostatic interactions in sheet formation, the ionic strength was varied. Sheet formation was observed above 500 mM NaCl and even up to 1 M, but the population of sheets was lessened significantly with increased ionic strength. The fact that high ionic strength did not abolish assembly suggests that hydrophobic interactions contribute significantly to sheet stability (Supplementary Fig. S8). The importance of hydrophobic interactions was supported by the observation that sheet formation did not take place in solutions containing over 50% acetonitrile (Supplementary B2).

Sheet formation is dependent on peptoid chain length. We synthesized a length series of charged pairs of 18, 12 and 6 residues: $[(Nae–Npe)_9$ and $(Nce–Npe)_9]$, $[(Nae–Npe)_6$ and $(Nce–Npe)_6]$ and $[(Nae–Npe)_3$ and $(Nce–Npe)_3]$. 18mer and 12mer peptoids produced sheets under typical conditions. However, the sheet-forming capability of the 12mer decreased significantly, and 6mer

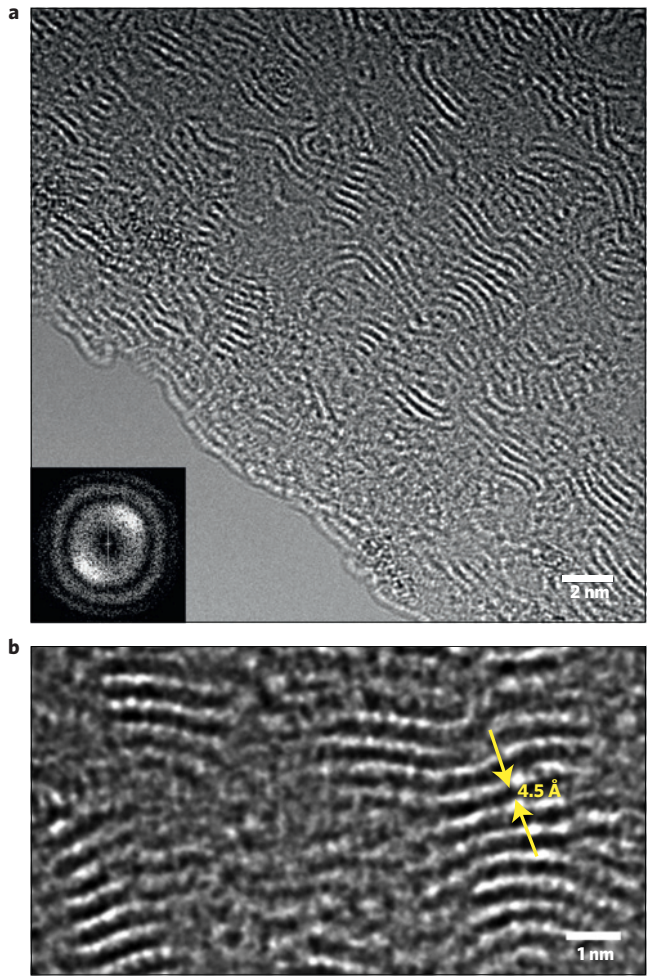

Figure 3 | Direct observation of peptoid chains using aberration-corrected TEM (TEAM 0.5). a, High-resolution TEM image of peptoids assembled into a sheet. Inset: Fourier transform of the image showing the alignment of peptoids along the sheet edge. **b**, Magnified image of the individual peptoids, fully extended along one direction in a sheet. TEAM 0.5 was operated at 80 kV with a third-order spherical aberration tuned to $Cs = -0.010$ mm. To decrease the energy spread of the incoming electron beam and consequently achieve sub-ångström resolution, the gun electron monochromator was inserted. As a negative value of the third-order spherical aberration was set in combination with a positive fifth-order spherical aberration, overfocusing yielded white-atom contrast.

peptoids did not assemble into sheets (Supplementary Fig. S9) unless the concentrations of $(Nae–Npe)_3$ and $(Nce–Npe)_3$ were higher than 5 mM. With each decrease in chain length, the contributions of the multiple weak interactions that drive sheet formation also decrease per molecule. The increase in chain-end effects and the smaller benefit of translational entropy increase on sheet formation are also probable factors for the weaker sheet-forming capability.

To understand the structural requirements needed to form sheets, analogues were synthesized and compared in terms of sheet-forming capability and kinetics. A neutral hydrophilic group, a methyl ether, was used to systematically replace the ionic and hydrophobic groups in turn. *N*-(2-methoxyethyl)glycine (Nme) was incorporated instead of Nce, Nae or Npe, making $(Nce–Nme)_{18}$, $(Nae–Nme)_{18}$ and $(Nme–Npe)_{18}$. None of the mixing combinations of these three sequences produced sheet-like structures (Supplementary Fig. S10). Through these control experiments, it can be concluded that both hydrophobic and electrostatic interactions play important roles. To probe the hydrophobic core, *N*-benzylglycine (Nbn) was used instead of Npe. The mixing of $(Nce–Nbn)_{18}$ and $(Nae–Nbn)_{18}$ produced crystalline sheets, but the population of sheets was reduced significantly and the kinetics of formation were slower. The decreased sheet-forming capability may be attributed to the benzyl groups having less conformational freedom to adopt an optimal packing geometry as well as less hydrophobicity overall. The thickness of the benzyl sheets was 2.5 nm, a decrease of 2 Å compared with the phenethyl sheets, according to the XRD (Supplementary Fig. S11).

Taken together, these observations and results allow us to propose a model for the peptoid sheet structure. To minimize the exposure of hydrophobic groups to water and to bring each cationic group next to an anionic group, the amphiphilic chains need to laterally align side-by-side in a fully extended conformation, where the side chains face up and down in an alternating pattern (Fig. 1c). Two such monolayers oppose one another to bury each hydrophobic face. This results in a bilayer structure consisting of a hydrophobic interior and two polar faces. It is likely that the neighbouring chains are not perfectly in register along their length axis, leaving protruding sticky ends that can adjoin the next strand. This model explains why the sheets are water soluble and can propagate their planar structure in two dimensions. The reduced sheet thickness in the case of $(Nce–Nbn)_{18}$ and $(Nae–Nbn)_{18}$ is due to the loss of two single carbon–carbon bonds, supporting our proposed geometry.

The mechanism of sheet formation was investigated by a variety of spectroscopic and microscopic techniques (Fig. 5). Sheet formation involves fast complexation of oppositely charged peptoids into an aggregated state followed by slow re-ordering of the peptoid chains into a crystalline sheet. Ordering of the peptoid chains is probably driven by maximizing aromatic pi–pi interactions, maximizing electrostatic attraction and minimizing the exposure of hydrophobic groups to water. The related phenomenon of the emergence of an ordered polymer structure from an initial amorphous aggregate has been described in the formation of peptide-based amyloid fibres[41]. When $(Nae–Npe)_{18}$ and $(Nce–Npe)_{18}$ are mixed at 0.1 mM, a cloudy solution is immediately produced. By monitoring the optical transmittance at 650 nm, the transition to a clear solution was observed over an 18-h period (Fig. 5e). Interestingly, the turbidity curve shows evidence of an initial 3-h lag phase followed by a distinct growth phase. This transformation was monitored in detail by fluorescence microscopy (Fig. 5a–c). Images were collected every hour between 1 and 12 h after mixing (Supplementary Fig. S12).

To better understand the sphere to sheet transition kinetics, we synthesized a pair of analogues where a hydrophilic Förster resonance energy transfer (FRET) reporter group was introduced in the place of an ionic residue at position 5. Thus, $(Nae–Npe)_{18}$ and $(Nce–Npe)_{18}$ were each site-specifically labelled with AlexaFluor 555 and AlexaFluor 647, respectively, and added to the peptoid solutions before mixing at 0.1% and 0.4% of the overall peptoid concentration. At this low level of dye incorporation, sheet formation was not affected, and the FRET efficiency is highly sensitive to changes in donor–acceptor distance caused by the bulk rearrangement of the peptoid chains (Fig. 5e). In the initial spherical aggregates formed on mixing, donor and acceptor dyes are on average much closer than when the material is spread out over two dimensions at a thickness of 2.7 nm. After a 3-h lag period, the initial FRET efficiency of 0.26 decreases exponentially to zero over the course of 20 h during the sheet growth phase. This bi-phasic behaviour directly matches the turbidity curve (Fig. 5e).

On initial mixing, hydrophobic collapse and Coulombic attraction contribute to rapid formation of spherical aggregates (Supplementary Fig. S13). Isothermal titration calorimetry experiments showed that this initial complexation is exothermic

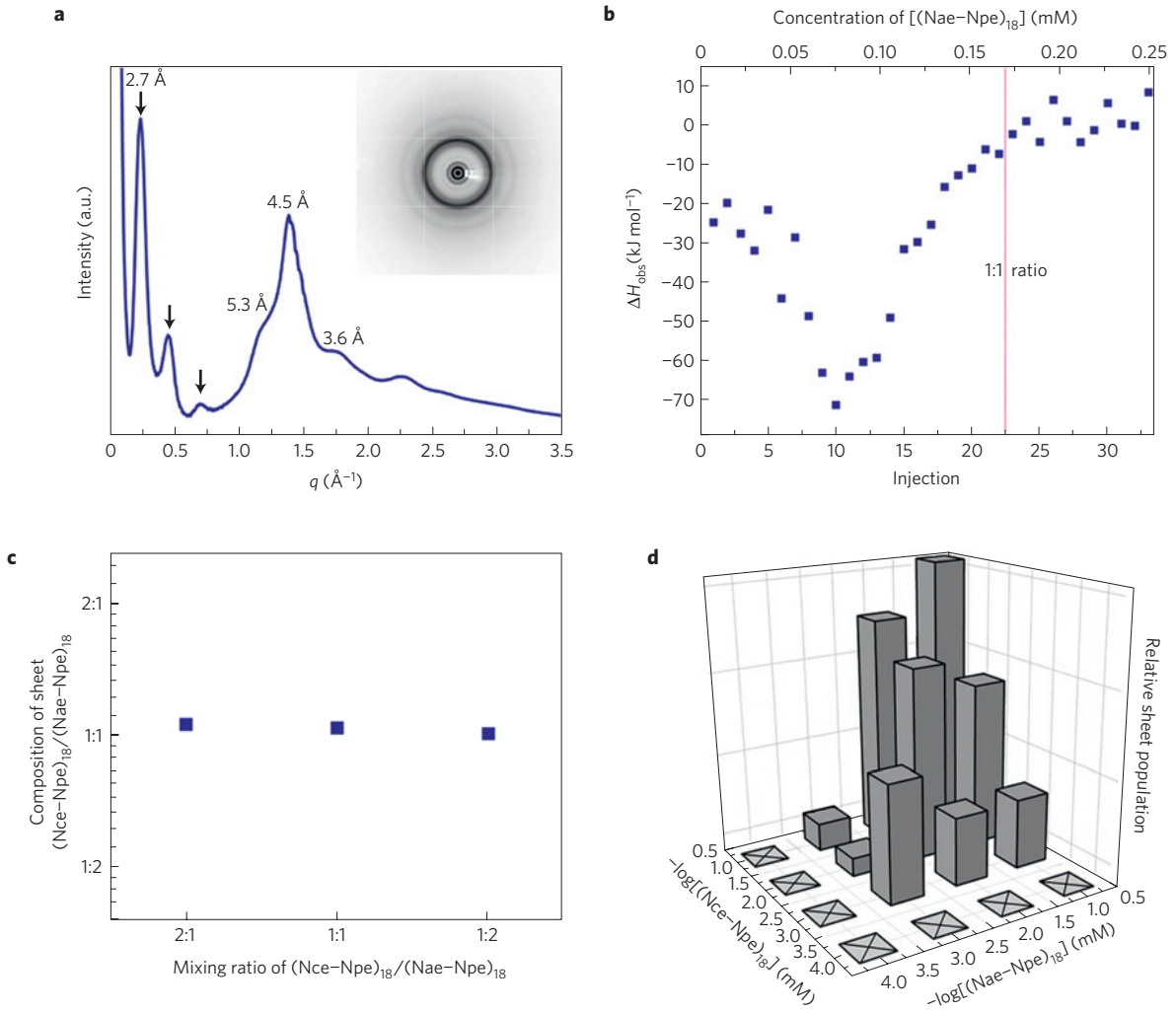

Figure 4 | Characterization of sheets and sheet-formation kinetics. a, XRD data from the sheets. The three equally spaced peaks marked by arrows indicate that the thickness of the sheet is 27 Å. The two peaks at 0.46 and 0.69 $Å^{-1}$ are lamellar harmonics of 27 Å. **b**, Isothermal titration calorimetry curve for the $(Nae–Npe)_{18}/(Nce–Npe)_{18}$ system. Five-microlitre aliquots of 1.8 mM $(Nae–Npe)_{18}$ were titrated into 0.2 mM of $(Nce–Npe)_{18}$. **c**, Composition of sheets prepared with different initial mixing ratios of $(Nae–Npe)_{18}$ and $(Nce–Npe)_{18}$. All resulting sheets contained a 1:1 ratio as determined by analytical high-performance liquid chromatography. **d**, The yield of sheet formation depends on the relative concentration of $(Nae–Npe)_{18}/(Nce–Npe)_{18}$. Sheet population scales with the surface coverage as measured by fluorescence microscopy. X indicates that there is no sheet formation. According to our estimation, for the sample containing 0.1 mM of $(Nae–Npe)_{18}$ and $(Nce–Npe)_{18}$, the yield of sheet formation is 64%.

(Fig. 4b and Supplementary Fig. S14). The initial complexes are about 200 nm in size and roughly triple in size in the next 20 min as evidenced by dynamic light scattering (Supplementary Fig. S15). Although sheets cannot be observed at this early stage, TEM analysis of the spheres after 30 min reveals that small amounts of sheet material are associated with each sphere (Fig. 5d). Facet-like features are also clearly visible in the spheres, suggesting that local ordering is already underway well before sheet formation. Further evidence that these early spheres are partially ordered is provided by powder XRD experiments, which showed broad and distinct peaks corresponding to a spacing of 2 nm and 4.5 Å (Supplementary Fig. S16).

At 4 h, just after the transition from the lag phase to the growth phase, the first isolated sheets begin to appear with their characteristic sharp edges as observed by SEM. The size of these early sheets is small, averaging less than 10 μm in length and 5 μm in width (Fig. 5f). As both the length and width edges of the sheet bilayer contain an exposed hydrophobic stripe of similar dimension, sheet growth can occur at similar rates in both planar dimensions.

One potential application of these nanosheet structures is to serve as chemically well-defined hydrophilic scaffolds on which biologically active ligands can be displayed for biomolecular recognition. To explore this possibility, we designed a modified version of the sheet-forming polymer in which the streptavidin-binding peptide ligand cyclo-[CHPQFC] (ref. 42) was appended to the *N*-terminus of the $(Nae–Npe)_{18}$ peptoid chain by means of a short hydrophilic linker (Fig. 6a). Mixing of this modified polypeptoid with normal $(Nce–Npe)_{18}$ produced sheets with identical morphology and comparable population (Fig. 6b). To confirm that the protein-binding ligand was displayed on the sheet surface as desired, binding experiments were carried out with fluorescently labelled streptavidin. Both ligand-bearing and normal sheets were mixed with Cy3–streptavidin and washed with buffer. The functionalized sheets retained significant Cy3 fluorescence (Fig. 6c), whereas the negative-control normal sheets had minimal fluorescence (<2% of the ligand-bearing sheets as determined by solution fluorescence) (Fig. 6d). This demonstrates that a biologically active ligand can be linked to a sheet-forming peptoid and still undergo self-assembly, and that the ligand is

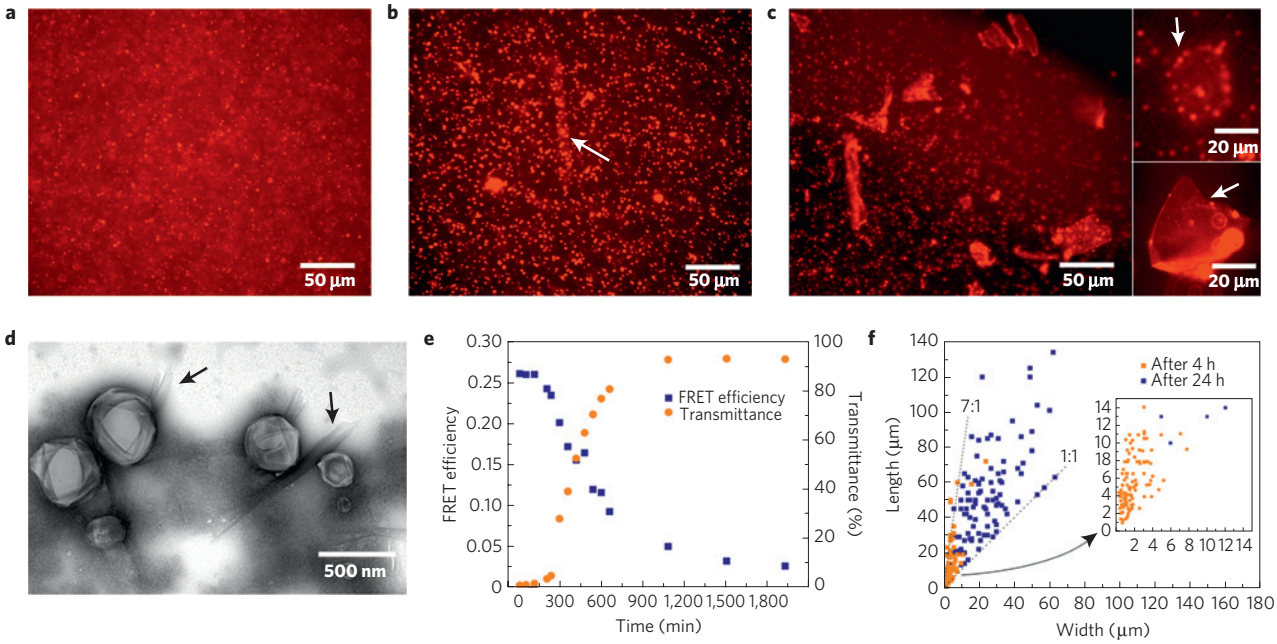

Figure 5 | Sheet-formation kinetics and mechanism. a, Fluorescence microscopy images of the cloudy solution 1 h after mixing of the two peptoids. Only spheres are observed. **b**, Four hours after mixing. Some spheres begin to organize in a planar sheet-like structure as pointed out by the white arrow. **c**, Six hours after mixing. Well-defined sheets associated with high concentrations of spheres are observed. **d**, TEM image of spheres found 30 min after mixing. The initial sheets protruding from spheres are pointed out by the black arrows. **e**, Study of sheet-formation kinetics using FRET efficiency and monitoring the transmittance change over time of 650 nm light through the solution. **f**, Size distribution of sheets at two time points measured by SEM and fluorescence microscopy.

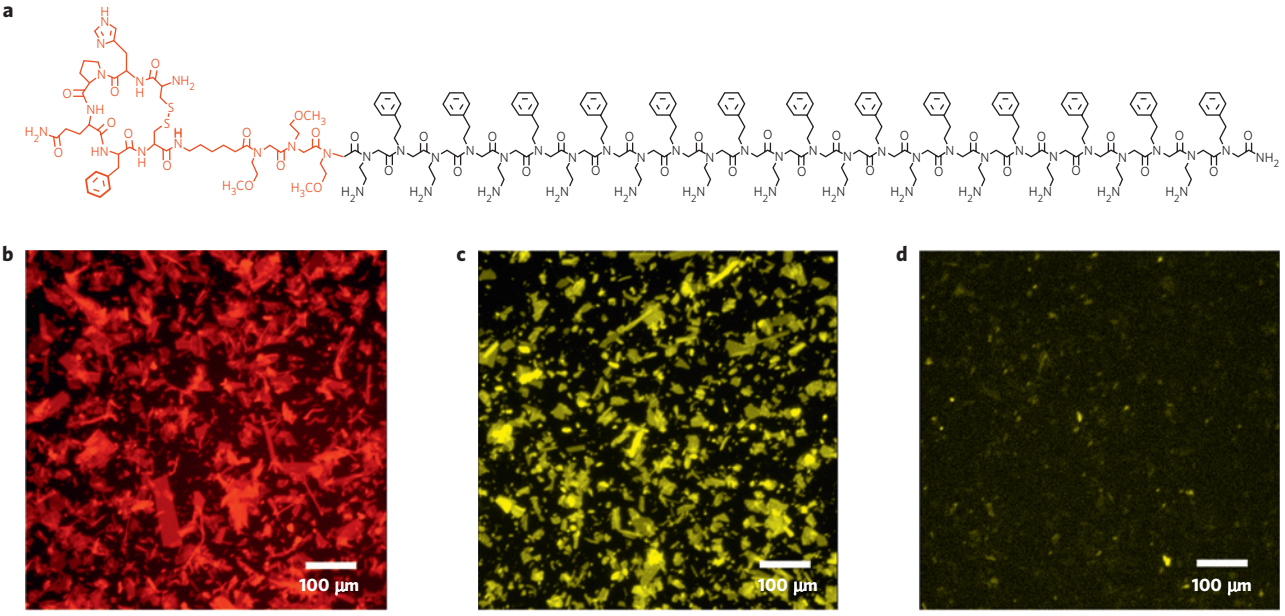

Figure 6 | Specific protein binding to functionalized sheets. a, The streptavidin-binding peptide sequence cyclo-[CHPQFC]- was incorporated at the *N*-terminus of the sheet-forming peptoid by means of a short hydrophilic linker. **b**, Self-assembly with the functionalized peptoid yields a similar population and morphology of nanosheets in comparison to un-functionalized peptoid as indicated by fluorescence microscopy using Nile Red. **c**, Ligand-bearing sheets show a high level of fluorescence after binding to Cy3–streptavidin. **d**, Un-functionalized sheets fluoresce very weakly under identical conditions and washes, indicating that binding to the modified sheets is specific.

displayed on the surface of the sheet and can specifically bind a protein of interest.

The biomimetic approach presented here for the spontaneous assembly of crystalline sheets has technological potential in the development of self-assembled devices that use 2D nanostructures. Surprisingly, the twofold periodic sequence pattern[28] observed in β-sheet-forming proteins can be translated to the assembly of non-natural peptoid polymers in spite of the structural differences between peptoids and proteins. The lack of hydrogen bonding in the peptoid system allows for the dynamic chain rearrangement and interdiffusion necessary for the thermodynamically favourable transition from the initial complex to crystalline sheets. Further-

more, achirality of the peptoid backbone enables the formation of untwisted, flat sheets that are laterally extended in two dimensions. These ultrathin 2D crystals improve on many aspects of other 2D materials—extremely high aspect ratio, ease of synthesis, site-selective functionalization and formation under physiological conditions. The ability to efficiently create functionalized 2D crystals by spontaneous assembly will lead to many applications in device fabrication, nanoscale synthesis and imaging, membrane mimetics, sensors and separations. More generally, the ability to mimic protein architecture with synthetic polymers should eventually enable new families of robust artificial proteins with highly specific functionality.

Full methods and any associated characterization methods are available in the Supplementary Information.

Received 17 August 2009; accepted 8 March 2010; published online 11 April 2010

References

1. Cornelissen, J. J. L. M., Rowan, A. E., Nolte, R. J. M. & Sommerdijk, N. A. J. M. Chiral architectures from macromolecular building blocks. *Chem. Rev.* **101,** 4039–4070 (2001).
2. Fredrickson, G. H. & Bates, F. S. Dynamics of block copolymers: Theory and experiment. *Annu. Rev. Mater. Sci.* **26,** 501–550 (1996).
3. Lin, Y., Skaff, H., Emrick, T., Dinsmore, A. D. & Russell, T. P. Nanoparticle assembly and transport at liquid–liquid interfaces. *Science* **299,** 226–229 (2003).
4. Percec, V. *et al.* Poly(oxazolines)s with tapered minidendritic side groups the simplest cylindrical models to investigate the formation of two-dimensional and three-dimensional order by direct visualization. *Biomacromolecules* **2,** 706–728 (2001).
5. Ulman, A. Formation and structure of self-assembled monolayers. *Chem. Rev.* **96,** 1533–1554 (1996).
6. Sakamoto, J., van Heijst, J., Lukin, O. & Schlüter, A. D. Two-dimensional polymers: Just a dream of synthetic chemists? *Angew. Chem. Int. Ed.* **48,** 1030–1069 (2009).
7. Dikin, D. A. *et al.* Preparation and characterization of graphene oxide paper. *Nature* **448,** 457–460 (2007).
8. Zhang, S. G., Holmes, T., Lockshin, C. & Rich, A. Spontaneous assembly of a self-complementary oligopeptide to form a stable macroscopic membrane. *Proc. Natl Acad. Sci. USA* **90,** 3334–3338 (1993).
9. Tang, Z. Y., Zhang, Z. L., Wang, Y., Glotzer, S. C. & Kotov, N. A. Self-assembly of CdTe nanocrystals into free-floating sheets. *Science* **314,** 274–278 (2006).
10. Gast, A. P., Vinson, P. K. & Coganfarinas, K. A. An intriguing morphology in crystallizable block copolymers. *Macromolecules* **26,** 1774–1776 (1993).
11. Keith, H. D., Giannoni, G. & Padden, F. J. Single crystals of poly(L-glutamic acid). *Biopolymers* **7,** 775–792 (1969).
12. Keller, A. A note on single crystals in polymers—evidence for a folded chain configuration. *Phil. Mag.* **2,** 1171–1175 (1957).
13. Bassett, D. C. *Principles of Polymers Morphology* (Cambridge Univ. Press, 1981).
14. Geil, P. H. *Polymer Single Crystal* (Wiley, 1963).
15. Nakamura, J. & Kawaguchi, A. *In situ* observations of annealing behaviour of polyethylene single crystals on various substrates by AFM. *Macromolecules* **37,** 3725–3734 (2004).
16. Brack, A. & Orgel, L. E. Beta-structures of alternating polypeptides and their possible prebiotic significance. *Nature* **256,** 383–387 (1975).
17. Zhang, S. G. Fabrication of novel biomaterials through molecular self-assembly. *Nature Biotech.* **21,** 1171–1178 (2003).
18. Aggeli, A. *et al.* Hierarchical self-assembly of chiral rod-like molecules as a model for peptide beta-sheet tapes, ribbons, fibrils, and fibers. *Proc. Natl Acad. Sci. USA* **98,** 11857–11862 (2001).
19. Krejchi, M. T. *et al.* Chemical sequence control of beta-sheet assembly in macromolecular crystals of periodic polypeptides. *Science* **265,** 1427–1432 (1994).
20. Vauthey, S., Santoso, S., Gong, H. Y., Watson, N. & Zhang, S. G. Molecular self-assembly of surfactant-like peptides to form nanotubes and nanovesicles. *Proc. Natl Acad. Sci. USA* **99,** 5355–5360 (2002).
21. Simon, R. J. *et al.* Peptoids—a modular approach to drug discovery. *Proc. Natl Acad. Sci. USA* **89,** 9367–9371 (1992).
22. Barron, A. E. & Zuckermann, R. N. Bioinspired polymeric materials: In-between proteins and plastics. *Curr. Opin. Chem. Biol.* **3,** 681–687 (1999).
23. Murphy, J. E. *et al.* A combinatorial approach to the discovery of efficient cationic peptoid reagents for gene delivery. *Proc. Natl Acad. Sci. USA* **95,** 1517–1522 (1998).
24. Kirshenbaum, K. *et al.* Sequence-specific polypeptoids: A diverse family of heteropolymers with stable secondary structure. *Proc. Natl Acad. Sci. USA* **95,** 4303–4308 (1998).
25. Lee, B. C., Chu, T. K., Dill, K. A. & Zuckermann, R. N. Biomimetic nanostructures: Creating a high-affinity zinc-binding site in a folded nonbiological polymer. *J. Am. Chem. Soc.* **130,** 8847–8855 (2008).
26. Zuckermann, R. N., Kerr, J. M., Kent, S. B. H. & Moos, W. H. Efficient method for the preparation of peptoids [oligo(*N*-substituted glycines)] by submonomer solid-phase synthesis. *J. Am. Chem. Soc.* **114,** 10646–10647 (1992).
27. Dill, K. A. Dominant forces in protein folding. *Biochemistry* **29,** 7133–7155 (1990).
28. Xiong, H. Y., Buckwalter, B. L., Shieh, H. M. & Hecht, M. H. Periodicity of polar and nonpolar amino-acids is the major determinant of secondary structure in self-assembling oligomeric peptides. *Proc. Natl Acad. Sci. USA* **92,** 6349–6353 (1995).
29. Minor, D. L. & Kim, P. S. Context is a major determinant of beta-sheet propensity. *Nature* **371,** 264–267 (1994).
30. Decher, G. Fuzzy nanoassemblies: Toward layered polymeric multicomposites. *Science* **277,** 1232–1237 (1997).
31. Hammond, P. T. Form and function in multilayer assembly: New applications at the nanoscale. *Adv. Mater.* **16,** 1271–1293 (2004).
32. Kaler, E. W., Herrington, K. L., Murthy, A. K. & Zasadzinski, J. A. N. Phase-behavior and structures of mixtures of anionic and cationic surfactants. *J. Phys. Chem.* **96,** 6698–6707 (1992).
33. Radler, J. O., Koltover, I., Salditt, T. & Safinya, C. R. Structure of DNA-cationic liposome complexes: DNA intercalation in multilamellar membranes in distinct interhelical packing regimes. *Science* **275,** 810–814 (1997).
34. Hong, Y. S., Legge, R. L., Zhang, S. & Chen, P. Effect of amino acid sequence and pH on nanofiber formation of self-assembling peptides EAK16-II and EAK16-IV. *Biomacromolecules* **4,** 1433–1442 (2003).
35. Oda, R., Huc, I., Schmutz, M., Candau, S. J. & MacKintosh, F. C. Tuning bilayer twist using chiral counterions. *Nature* **399,** 566–569 (1999).
36. Hunter, C. A., Lawson, K. R., Perkins, J. & Urch, C. J. Aromatic interactions. *J. Chem. Soc. Perkin Trans.* **2,** 651–669 (2001).
37. Pedersen, J. S. Form factors of block copolymer micelles with spherical, ellipsoidal and cylindrical cores. *J. Appl. Cryst.* **33,** 637–640 (2000).
38. Kisielowski, C. *et al.* Detection of single atoms and buried defects in three dimensions by aberration-corrected electron microscope with 0.5-angstrom information limit. *Microsc. Microanal.* **14,** 469–477 (2008).
39. Sui, Q., Borchardt, D. & Rabenstein, D. L. Kinetics and equilibria of *cis*/*trans* isomerization of backbone amide bonds in peptoids. *J. Am. Chem. Soc.* **129,** 12042–12048 (2007).
40. Glaeser, R. in *Physical Aspects of Electron Microscopy and Microbeam Analysis* (eds Siegel, B. M. & Beaman, D. R.) Ch. 12 (Wiley, 1975).
41. Carullaa, N. *et al.* Experimental characterization of disordered and ordered aggregates populated during the process of amyloid fibril formation. *Proc. Natl Acad. Sci. USA* **106,** 7828–7833 (2009).
42. Giebel, L. B. *et al.* Screening of cyclic peptide phage libraries identifies ligands that bind streptavidin with high affinities. *Biochemistry* **34,** 15430–15435 (1995).

Acknowledgements

We thank P. Ashby, S. Whitelam and J. Schmit for helpful discussions and S. Yakovlev and K. Downing for help with electron diffraction. We acknowledge J. Holton and G. Meigs for all of their support at beamline 8.3.1 and E. Schaible and A. Hexemer for solution X-ray scattering experiments at beamline 7.3.3 at the Advanced Light Source and Claire Woo for grazing-incidence XRD data. This work was carried out at the Molecular Foundry, the National Center for Electron Microscopy and the Advanced Light Source at Lawrence Berkeley National Laboratory, all of which are supported by the Office of Science, Office of Basic Energy Sciences, of the US Department of Energy under Contract No. DE-AC02—05CH11231. L.T. and P.H.C. were supported by the Defense Threat Reduction Agency (IACRO-B0845281).

Author contributions

K.T.N. and R.N.Z. designed research and wrote the paper. K.T.N., S.A.S., A.B.M., P.H.C., R.C. and L.T. carried out analytical experiments. T.K.C., R.A.M, B-C.L. and M.D.C. carried out chemical synthesis. C.K. carried out the aberration-corrected TEM. All authors discussed the results and commented on the manuscript. R.N.Z. guided all aspects of the work.

Additional information

The authors declare no competing financial interests. Supplementary information accompanies this paper on www.nature.com/naturematerials. Reprints and permissions information is available online at http://npg.nature.com/reprintsandpermissions. Correspondence and requests for materials should be addressed to R.N.Z.